frontiers | Frontiers in Materials

TYPE Original Research
PUBLISHED 25 September 2025
DOI 10.3389/fmats.2025.1688171

OPEN ACCESS

EDITED BY
Xiangchen Meng,
Harbin Institute of Technology, China

REVIEWED BY
Nan Xu,
Hohai University, China
Hongbo Xia,
Yangzhou University, China
Jianfeng Wang,
Nanjing University of Aeronautics and Astronautics, China

*CORRESPONDENCE
Xueqing Hu,
hu_xueqing0322@163.com
Wunian Wang,
wangwunian@ujs.edu.cn

RECEIVED 18 August 2025
ACCEPTED 08 September 2025
PUBLISHED 25 September 2025

CITATION
Hu X, Zhao W, Zhu Q and Wang W (2025) Achieving high-performance laser welding of SiCp/Al composites for lightweight sports equipment.
Front. Mater. 12:1688171.
doi: 10.3389/fmats.2025.1688171

Achieving high-performance laser welding of SiCp/Al composites for lightweight sports equipment

Xueqing Hu[1]*, Wentao Zhao[2], Qiang Zhu[2] and Wunian Wang[1]*

[1]Sports Department, Jiangsu University, Zhenjiang, China, [2]School of Materials Science & Engineering, Jiangsu University, Zhenjiang, China

Lightweight and high strength are key objectives in the development of sports equipment. Although aluminum alloys are still widely used as the primary material, they are limited by relatively low strength and inadequate wear resistance. To further improve the overall performance of sports products, advanced materials are required for their design and manufacture. Silicon carbide particle-reinforced aluminum matrix composites offer a promising alternative due to their high specific strength and stiffness, superior wear and corrosion resistance. These properties make them well-suited for applications demanding lightweight and high-strength characteristics in sports equipment. This study examined the laser welding quality of silicon carbide particle-reinforced aluminum matrix composites fabricated using two distinct methods. The suppression of brittle phases, control of porosity defects, and reinforcement mechanisms at the welded joint were systematically explored through advanced process including continuous laser welding, ultrasonic-assisted laser welding, and the application of active interlayers. It was demonstrated that the continuous laser welding process with addition an active interlayer effectively enhanced molten pool fluidity, thereby minimizing SiC particle burn-off and inhibiting the formation of Al_4C_3 brittle phases. A joint tensile strength exceeding 80% of the base material was consequently achieved. This research provides an efficient joining technology solution for sports equipment manufacturing, facilitating the broader application of lightweight composite materials in high-end sporting goods.

KEYWORDS

aluminum matrix composites, laser welding, defects formation, ultrasonic, metallurgical strengthening

1 Introduction

The sports equipment manufacturing industry is undergoing a technological transformation towards lighter weight and higher performance. Aluminum alloys, prized for their high specific strength (strength-to-density ratio) and excellent corrosion resistance, have become core materials for premium equipment like competition-grade bicycles, tennis racket frames, and mountaineering gear (Chen, 2024). Replacing traditional steel with aluminum alloys can reduce structural weight by over 50%, significantly enhancing equipment handling

performance (Leng et al., 2024; Wang et al., 2025). However, the strength and wear resistance of conventional aluminum alloys often fall short under the extreme operating conditions demanded by competitive sports equipment (Ferraris et al., 2022; Sun et al., 2023).

This challenge has spurred the development of aluminum matrix composites (AMCs). Compared to conventional aluminum alloys of the same specification, AMCs offer superior specific strength, specific stiffness, enhanced high-temperature mechanical properties, lower coefficients of thermal expansion, and improved wear resistance (Singh et al., 2021; Madhu et al., 2025). These advantages make them highly promising for aerospace, aviation, automotive, shipbuilding, and defense applications. By incorporating 5%–50% by volume of silicon carbide (SiC) particles into the aluminum matrix, these composites achieve increased tensile strength and wear resistance while maintaining a favorable low density. In professional sports, components like bicycle suspension frames made from such composites can withstand over 10^5 cycles of impact loading without failure, and badminton racket string groove wear life is extended by 100% (Barker et al., 2020; Zhou and Zhang, 2023). The conventional fabrication techniques for aluminum matrix composites (AMCs) typically involve both solid-state processes, such as powder metallurgy and friction stir processing, and liquid-state processes, including stir casting and compo casting (Ndukwe, 2023; Sharma et al., 2021; Hao et al., 2023). Key AMC systems currently developed contain SiC_p/Al, Ti-B/Al, Al_2O_3/Al and SiCw/Al (Gupta et al., 2024; Xie et al., 2025; Lu et al., 2024). Among these, silicon carbide particle-reinforced aluminum composites (SiCp/Al) stand out due to their relatively lower cost and simpler processing routes compared to alternatives (Chatterjee et al., 2023). This combination makes SiCp/Al composites the most promising candidate for cost-effective, large-scale industrial production, solidifying their position as the most competitive and widely recognized metal matrix composites today.

Despite their superior properties, SiCp/Al composites face critical barriers to widespread use in sports equipment manufacturing primarily due to the inherent weldability challenges stemming from their multiphase and heterogeneous structure (Kesharwani et al., 2024). The significant physical and chemical property differences between the aluminum matrix and the SiC reinforcement phase complicate interfacial behavior during welding (Zhang et al., 2024a). The aluminum matrix itself is a ductile and tough metal and is generally weldable. However, the SiC reinforcement phase exhibits poor weldability, characterized by high strength, high elastic modulus, high melting point, and low coefficient of thermal expansion. This fundamental mismatch makes controlling the welding performance of aluminum matrix composites exceptionally difficult, hindering their industrial-scale application.

Interfacial reactions between SiC and the aluminum matrix, triggered by conventional fusion welding, generate brittle and acicular Al_4C_3 phases. Due to its hygroscopic nature, this phase caused corrosive cracking in welded joint and reduced joint strength to less than 40% of the base material's strength (Gao et al., 2025). Furthermore, the remelting process in weld seam may cause SiC particle segregation, resulting in uneven particle distribution and diminished reinforcement efficiency. The extremely high viscosity and poor fluidity of SiCp/Al molten pool readily led to defects like porosity and shrinkage cavities. Porosity rates can reach as high as 15%, and susceptibility to hot cracking was significantly increased (Pan et al., 2024). Joining complex and contoured structures common in sports equipment, particularly integrated bicycle frames, demands precisely controlled heat input. Conventional arc welding techniques induce excessive distortion, rendering them unsuitable for these applications.

Friction stir welding techniques can effectively mitigate these issues. However, this technique is often constrained by high equipment costs, the need for workpiece rigidity, and difficulties in joining complex or large-scale geometries. Laser welding offers high precision, speed, and minimal heat effect, which is a promising welding technique for metal matrix composites. A systematic review of the literature revealed that laser welding, including keyhole mode welding, beam offset welding, and pulsed welding, represents the predominant method for joining SiCp/Al composites (Zhang et al., 2024b; Li et al., 2025). The core challenge lied in synergistically suppressing the formation of detrimental Al_4C_3 brittle phases and enhancing joint performance through process optimization and interlayer design (Wang et al., 2023a). Zhang et al. (2022a) demonstrated that high-power, high-speed laser parameters (e.g., 7–9 kW at 6.0 m/min) could significantly reduce Al_4C_3 formation by minimizing high-temperature dwell time. Furthermore, employing an open keyhole mode and laser beam offset techniques optimized SiC particle distribution and refined grain structure by controlling molten pool flow dynamics (Zhang et al., 2024c; Zhang et al., 2023a). Studies have identified that fracture initiation in laser-welded joints of aluminum matrix composites typically occurs at unmelted SiC particles and weld porosity (Zhang et al., 2024b). Crucially, cracks propagated rapidly along the radial direction of acicular phases and through porosity within the weld seam, ultimately leading to joint failure.

In addition, active interlayer reinforcement is predominantly employed as the research strategy. The titanium-based materials (foils, powders, or sheets typically ranging from 0.04–0.3 mm in thickness) formed the core approach. The underlying mechanism relied on elements such as titanium and zirconium, which were selected for their elevated carbon affinity. These elements preferentially reacted with SiC, resulting in the formation of stable TiC and ZrC phases in composite system (Mi et al., 2021; Guo et al., 2012; Zhu et al., 2021). This effectively blocked the detrimental reaction chain ($4Al + 3SiC \rightarrow Al_4C_3 + 3Si$), while simultaneously enabling the *in situ* formation of strengthening phases such as $L1_2$-$(Al, Si)_3Ti$ and TiC (Zhang et al., 2023b). Composite filler materials (e.g., TiB_2/2024Al) could also help mitigate porosity defects (Zhang et al., 2024b; Han et al., 2025). This process involved a triple strengthening mechanism (Hua et al., 2024): Orowan strengthening induced by nano-scale TiC/ZrC particles, load transfer facilitated by stress-bearing carbide particles, and enhanced grain boundary strengthening due to the refined microstructure. Through these optimizations, joint strength can reach 75%–86% of the base material strength.

Although extensive research existed on the laser welding of SiCp/Al composites, direct comparisons were hindered by substantial variations in material systems and processing parameters. The successful laser welding of SiCp/Al composites was fundamentally attributed to elemental competition suppressing brittle phase formation and molten pool flow control ensuring reaction homogeneity. Hence, ultrasonic field assistance represented

TABLE 1 Mechanical properties of Al matrix composite.

type	Volume	Supply condition	Tensile strength (MPa)
SiCp/6092Al	17%vol	T6	459
SiCp/6061Al	17%vol	T6	356

TABLE 2 Chemical composition of Al matrix (wt%).

Composite	Mg	Cu	Si	O	Fe	Ti	Mn	Zn	Al
6092	0.9	0.8	0.6	0.05	0.7	0.15	—	—	Bal
6061	0.8~1.2	0.15~0.4	0.4~0.8	—	0.7	0.15	0.15	0.25	Bal

a promising strategy for enhancing the weld quality of composite (Li et al., 2021; Gao et al., 2020). Yet, research specifically on ultrasonically assisted welding remained limited. To address this gap, two distinct aluminum matrix composites—SiCp/6,092 produced via powder metallurgy and SiCp/Al6061 fabricated by stir casting—will be systematically evaluated in this paper to assess their feasibility for sports equipment applications. Microstructural characteristics and mechanical properties of laser-welded joints produced by three methods: direct laser welding, titanium-activated laser welding, and ultrasound-assisted laser welding, were investigated. This research is expected to facilitate the broader industrial adoption of aluminum matrix composites within the sports equipment sector.

2 Materials and methods

Two grades of SiCp/Al composites commonly employed in sports equipment were selected as the base materials. The SiCp/6092Al composite was fabricated via powder metallurgy with dimensions of 150 × 80 × 2 mm while the SiCp/6061Al composite was produced by stir casting with dimensions of 150 × 80 × 3 mm. In both composites, the reinforcement phase consisted of α-SiC particles (particle size: 5–7 μm, purity >99.9%). The mechanical properties and chemical compositions of the two composite systems are presented in Tables 1, 2, respectively. Representative metallographic micrographs of both are provided in Figure 1.

The laser welding trials were conducted using a TRUMPF TruDisk 6,002 disk laser (wavelength: 1.03 μm) manufactured in Germany. Three different welding procedures were employed for comparative analysis, as given in Figure 2. Firstly, the SiCp/6092Al and SiCp/6061Al composites were welded under same parameters (laser power: 2,000 W; travel speed: 0.022 m/s, defocusing distance: 0 mm). Weld bead morphology, defects formation and microstructural evolution were systematically compared to determine the composite suitable for sports equipment applications.

For the selected composite, two auxiliary techniques, including reactive-element assisted laser welding and ultrasound-assisted laser welding, were used to enhance the weld quality. During ultrasonic-assisted laser welding, ultrasonic were applied to the fixture and transmitted indirectly to the specimen. The ultrasonic horn remained stationary, positioned such that the distance between its central axis and the specimen edge was 10 mm. The ultrasonic vibration system operated at a frequency of 20 kHz with a maximum amplitude of 25 μm. During welding, the ultrasonic amplitude was set to 30%, 50%, and 80% of the maximum value.

Following welding, metallographic specimens (4 × 10 mm) were sectioned perpendicular to the weld direction using wire electrical discharge machining (EDM). Specimens were ground, polished and etched with the Keller's reagent. Microstructural and defect analysis of the composite laser-welded joints were performed according to the following procedure. Optical microscopy (OM) was employed to examine internal defects and Al_4C_3 phase distribution. Elemental distribution within the weld zone was determined using an FEI Nova Nano 450 field emission scanning electron microscope (FE-SEM) equipped with energy-dispersive X-ray spectroscopy (EDS). Phase distribution in welded joints was analyzed via electron backscatter diffraction (EBSD). Tensile specimens were prepared in accordance with GB/T 2651–2008. Tensile strength was measured using an Instron 5,985 universal testing machine. Tensile testing specimen dimensions are illustrated in Figure 3.

3 Results and discussion

3.1 Influence of aluminum matrix composite type on laser-welded joint quality

The typical cross-section of the laser-welded SiCp/6092Al joint is shown in Figure 4a. Significant porosity was observed in both fusion and heat-affected zones. Figure 4b displays that pores measuring up to 100 μm in diameter were detected in the heat-affected zone, substantially reducing joint's mechanical performance. Acicular phases were uniformly distributed in weld zone while gas pores were concentrated in the partially melted zone. Irregular pores along the fusion boundary formed a distinct ring-shaped porosity zone. Increased pore size and irregular morphology were noted near the upper weld surface. This porosity

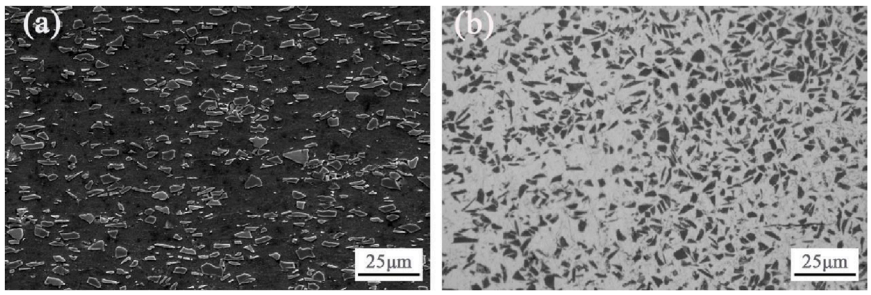

FIGURE 1
Microstructure of Al matrix composite **(a)** SiCp/6092Al, **(b)** SiCp/6061Al.

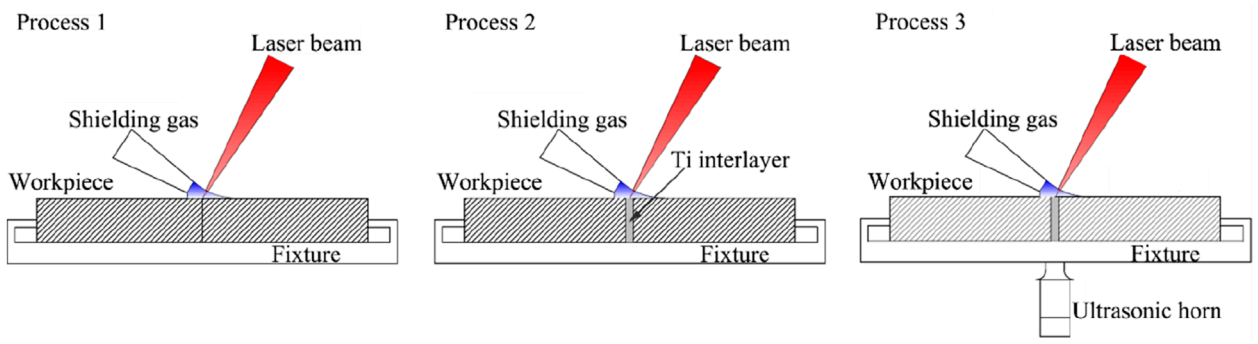

FIGURE 2
Three different laser welding process used in the present study.

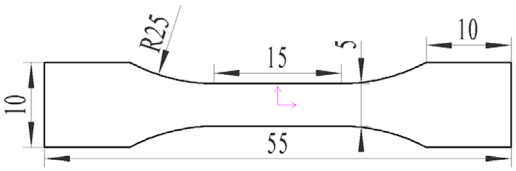

FIGURE 3
Dimensions of tensile specimens.

pattern originated from hydrogen release in supersaturated molten aluminum. Gas bubbles nucleated and expanded during welding. Buoyancy-driven detachment occurred when surface adhesion was overcome. It was difficult for gas to escape from this zone because rapid solidification combined with SiC-induced viscosity elevation created viscous resistance. Simultaneously, minor SiC particle segregation was found near the fusion boundary in partially melted regions. Poor wettability between unreacted SiC particles and Al matrix facilitated particle pushing during solidification front advancement, producing localized segregation. Additionally, a significant number of interlaced needle-like phases are observed within the weld metal (Figure 4c). The presence of such coarse microstructural features can significantly compromise the joint's properties.

Figure 5 presents the cross-sectional macrograph of a direct laser-welded joint in 6,061 aluminum matrix composites. Full penetration was achieved using the established process parameters. Compared to the 6,092 composite welded joints, fewer voids and gas pores were found in the heat-affected zone. However, segregated SiC particles were also present in the partially melted zone. This segregation causes increased viscosity during welding. Gas escape was consequently prevented, forming porosity defects. In weld metal, numerous acicular phases were distributed. Inadequate bonding between these phases was noted. This condition negatively impacted joint performance. Importantly, both this study and prior research indicate that pore and acicular phase defects cannot be eliminated solely through laser parameter optimization. Metallurgical modification using reactive elements was required. Such modification enabled defect reduction and joint performance enhancement in aluminum matrix composites.

3.2 Influence of Ti addition on laser-welded joint quality

Figure 6a shows the cross-section for a 6092 Al matrix composite joint welded with a 0.05 mm Ti interlayer. It can be observed that the porosity in central weld zone was essentially eliminated by the Ti foil addition. A significant reduction in the heat-affected zone (HAZ) width was also found. Figure 6b demonstrates that, a certain number

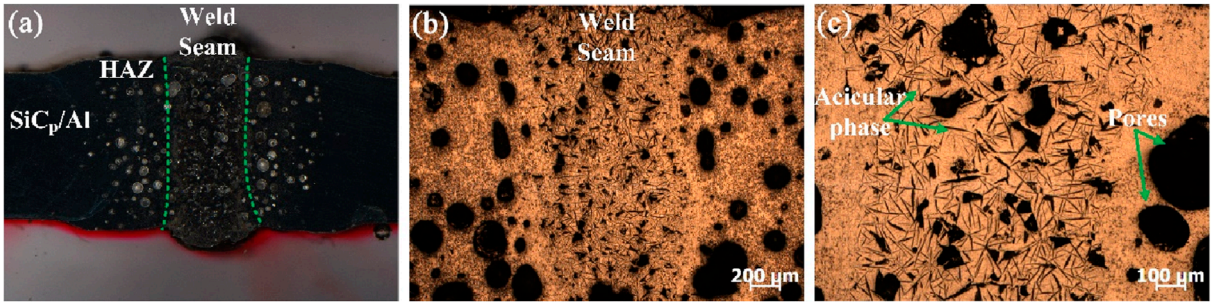

FIGURE 4
The typical SiCp/6092Al laser welded joint **(a)** Macrographic picture of cross-section, **(b)** Micrographic picture of cross-section, **(c)** acicular structure in weld zone.

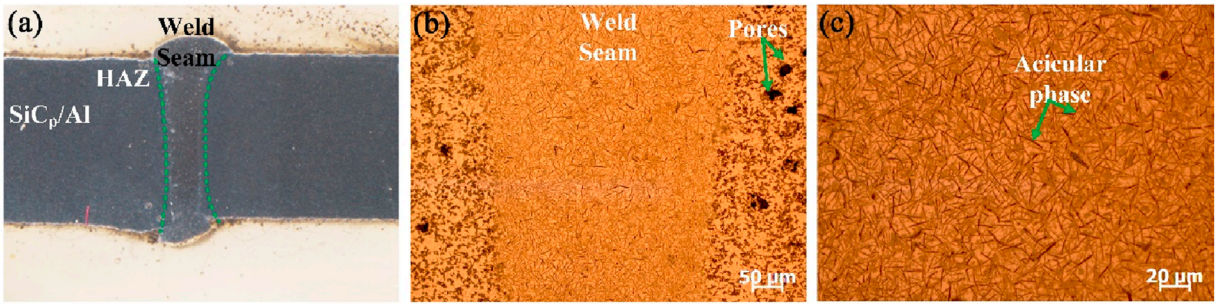

FIGURE 5
The SiCp/6061Al laser welded joint **(a)** Macrographic picture of cross-section, **(b)** Micrographic picture of cross-section, **(c)** acicular structure in weld zone.

of pores still remained in the HAZ. Both the volume and number of these residual pores were significantly reduced compared to joints produced by direct laser welding without Ti filler. The addition of Ti foil also promoted the formation of new TiC particulate phases. This occurred because Ti exhibited a stronger affinity for C than Al did. Consequently, the number of acicular brittle phases was markedly decreased relative to the condition without filler material as shown in Figure 6c. Overall, the presence of pores within the HAZ still results in relatively low joint performance when Ti foil is added. Due to the fact that the 6,092 composite material in this study was made by hot pressing sintering, the material was relatively loose and prone to porosity. This is in agreement with the research by Han et al. (2024). Therefore, the 6,092 aluminum based composite material in this study was difficult to use in sports equipment unless integrated molding or solid-phase joining methods are used (Huang et al., 2025; Meng et al., 2021).

Figure 7 illustrates the microstructural evolution in SiCp/6061Al composite welded joint with Ti interlayer. As can be seen from Figures 7a,b, significant changes have occurred in the composite laser-welded joint. The issue of weld porosity has essentially disappeared. It was visible in Figure 7c that the Al_4C_3 size was also decreased due to the introduction of Ti. The heat input of laser beam on composite was reduced due to the melting heat absorption of Ti filler. Carbon in molten pool preferentially also reacted with titanium, leading to the formation of fine and dispersed Ti-C particles. These particles served as heterogeneous nucleation sites for subsequent crystallization, thereby significantly reducing the Al_4C_3 size and markedly improving porosity defects in the weld. As depicted in Figure 7d, although acicular Al_4C_3 remained present when a 0.05 mm Ti layer was employed, a substantial refinement in its size was achieved. Simultaneously, Al_4C_3 precipitation was now confined solely to localized regions in the weld. The newly formed strengthening particles in the weld were identified as TiC, as corroborated by relevant research. During the crystallisation of aluminium alloys, TiC particles accumulate at grain boundaries and are subsequently displaced by the approaching solidification front, leading to TiC particle segregation. In addition, Zhao reported that excessive Ti content in the weld metal led to reactions with the aluminum matrix, forming a flaky phase identified as Al_3Ti based on related studies (Zhu et al., 2021). These results collectively demonstrated the effectiveness of Ti addition in suppressing interfacial reactions. However, insufficient diffusion of melted Ti throughout the entire molten pool occurred due to rapid solidification, causing localized Ti-C segregation.

Figure 8 presents EBSD analysis results of fusion boundary region in continuously laser-welded SiCp/6061Al composites with and without Ti addition. The EBSD band contrast map in Figures 8a, b provided a clear visualization of the sample microstructure. The imaging area of the EBSD map was the same as that in Figures 5, 7. Significant acicular phase formation and

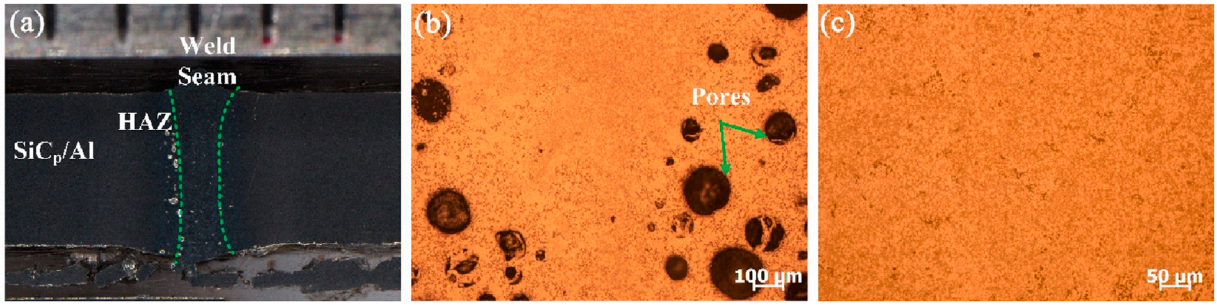

FIGURE 6
The SiCp/6092Al laser welded joint with Ti addition **(a)** Macrographic picture of cross-section, **(b)** picture of cross-section, **(c)** acicular structure in weld zone.

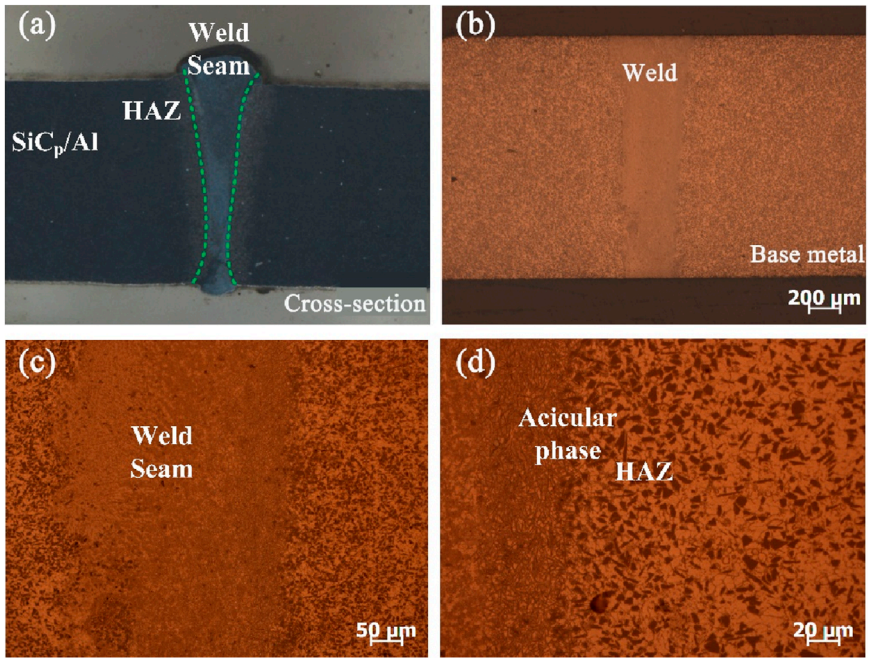

FIGURE 7
The SiCp/6,061 Al laser welded joint with Ti addition **(a)** Macrographic picture of cross-section **(b)** Micrographic picture of cross-section, **(c)** microstructure in weld zone, **(d)** acicular structure in HAZ.

porosity defects were produced in welds when no Ti was added. The corresponding phase images with and without Ti addition were depicted in Figures 8c,d. The main phases in the composite joints contained Al matrix, Al_4C_3, TiC and SiC. It was predicted that titanium preferentially reacted with SiC particles in molten pool to form TiC particles. Meanwhile, heat input was partially absorbed by the melting Ti foil, effectively suppressing pores formation and acicular phase development. Inverse pole figure (IPF) near the fusion boundary after Ti addition are provided in Figures 8e,f. These reveal the presence of TiC phases along with minor acicular Al_4C_3 phases following the introduction of 0.05 mm titanium. Notably, an anisotropic texture was observed in the joint, which was considered beneficial for enhancing mechanical properties. The random distribution of colors, without any dominant shade, suggests that there was no preferential grain orientation. Additionally, grain refinement was promoted by Ti addition, thereby further improving joint mechanical performance.

Figure 9 displays elemental mapping results in the weld center when 0.05 mm Ti foil was used. The weld center displayed no acicular reaction phases, having undergone complete replacement by uniformly substantially finer and near-spherical particles. Figures 9a–c indicated that the white particulate phases consist predominantly of Ti and C, identifying them as TiC phases. In contrast, Al and Si predominated in the grey matrix (Figures 9d,e). Ti addition was expected to form Ti-Al and Ti-Si compounds in weld metal. Notably, however, such compounds were undetected here, which was attributed to insufficient Ti content for reaction with Al and Si.

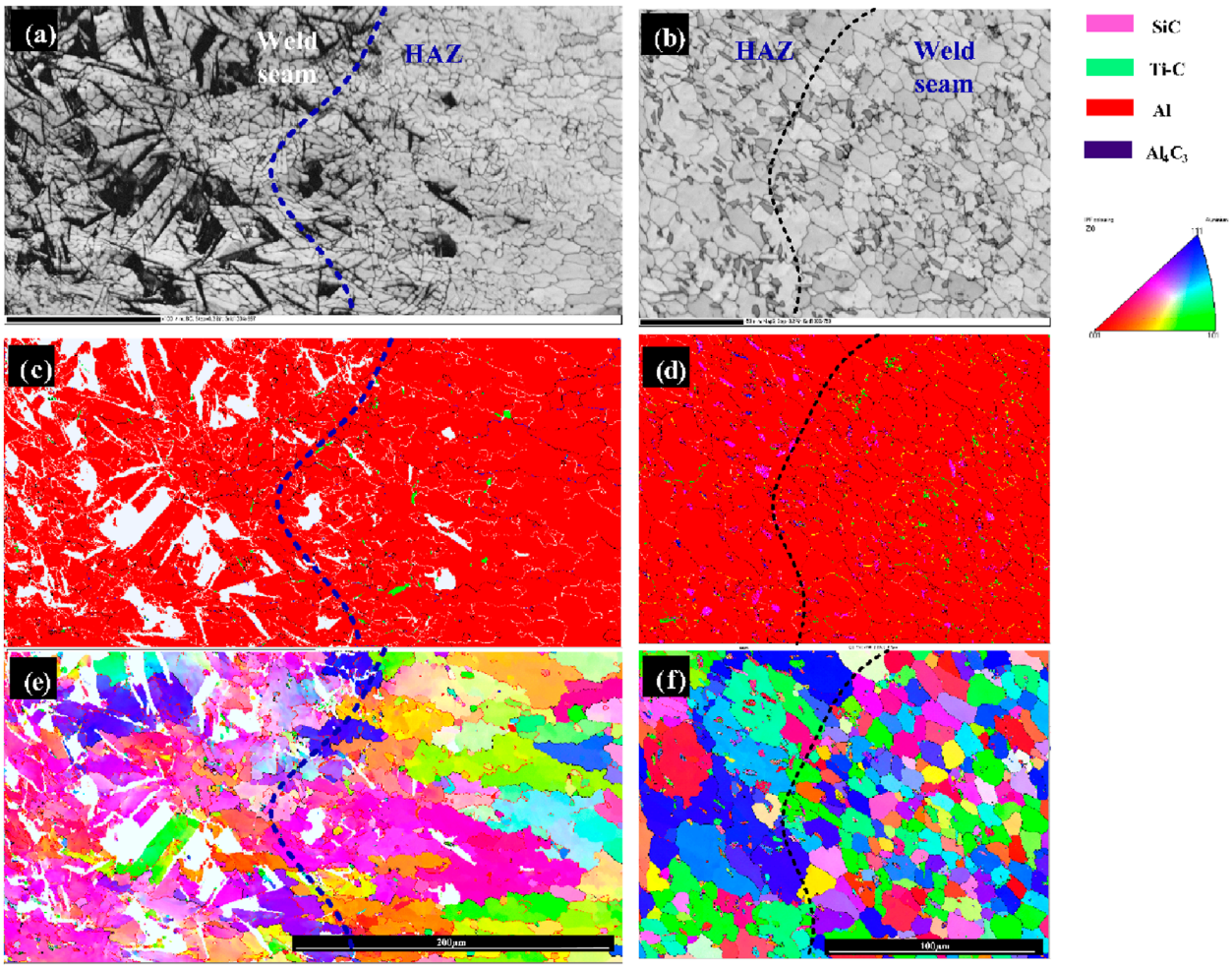

FIGURE 8
EBSD IPFs and phase distribution of the 6,061 composite laser welded joint: **(a)** EBSD band contrast map, **(c)** phase distribution and **(e)** IPFs of welded without Ti addition. Respectively. **(b)** EBSD band contrast map, **(d)** phase distribution and **(f)** IPFs of welded with Ti addition. Respectively.

3.3 Effects of ultrasound introduction on joint quality

Figure 10 presents the morphology of ultrasonic-assisted laser-welded joints for SiCp/6061Al matrix composites under different ultrasonic amplitudes. It was important to note that incorporating a 0.05 mm Ti foil failed to completely suppress acicular phase formation in weld center. The macroscopic morphologies of welds produced under 30%, 50%, and 80% ultrasonic vibration amplitudes are shown in Figures 10a1,b1,c1, respectively, with corresponding low-magnification metallographic cross-sections provided in Figures 10a2,b2,c2. These images revealed distinct variations in pore formation and acicular phase dimensions. Pore number and size exhibited a positive correlation with increasing ultrasonic amplitude. Welds produced at 30% were pore-free. At 80% amplitude, a high pore density was observed in both the weld zone (WZ) and partially melted zone (PMZ). Liu et al. stated that the small molten pool characteristic of laser welding combined with its rapid cooling rate becomes susceptible to pore formation under excessive ultrasonic vibration (Liu et al., 2019). Intense cavitation entraped significant volumes of metal vapor within the melt. This entrapped vapor cannot be fully escaped during the short solidification time, leading to internal pore formation that compromises weld quality and mechanical properties. Concurrently, Figures 10c1,c2,c3 acicular phase size increased from ~40 μm to 100 μm at high amplitude, substantially hindering performance enhancement.

Figure 11 shows metallographic images of the upper and middle weld regions under no ultrasound, 30% ultrasonic amplitude, and 80% ultrasonic amplitude conditions. Obviously, the acicular phase size in upper region was larger than that in the middle region because of the longer high-temperature dwell time of molten pool in the upper region. As depicted in Figures 11a,b,c, ultrasound had negligible impact on Al_4C_3 brittle phase structure in upper region for 0% and 30% amplitude. However, at 80% amplitude, the acicular phase size increased significantly (~50–60 μm) primarily due to ultrasonic thermal effects. Li et al. pointed that cavitation effect, particle collision, and particle friction induced by ultrasonic vibration would convert mechanical energy into thermal energy (Linjie et al., 2024). That is, with the continuous application of

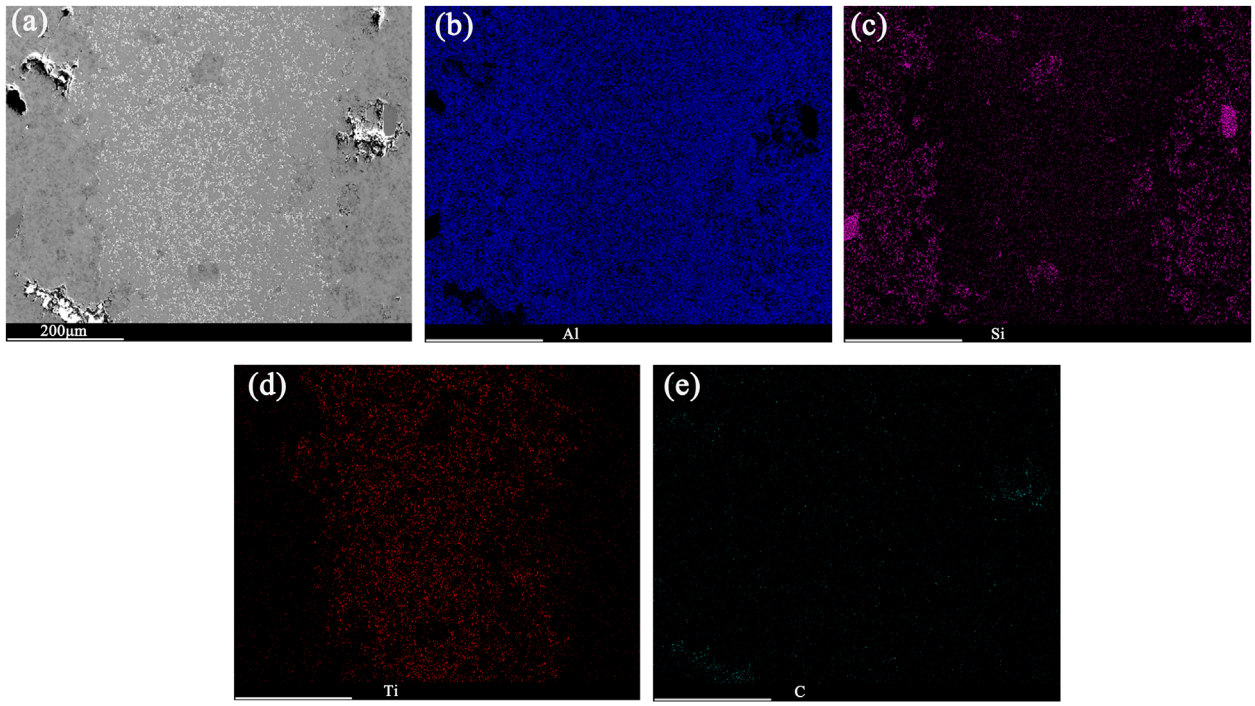

FIGURE 9
EDS mapping of the weld metal with Ti addition. **(a)** SEM image of the weld metal, **(b–e)** corresponding elemental distribution of Ti, Si, Al and C, respectively.

ultrasonic field, the high temperature dwell time of weld zone may decrease. Compared with acicular phases in Figure 11b, the Al_4C_3 phases formed at 30% ultrasonic amplitude were significantly finer, as shown in Figure 11d. Notably, Al_4C_3 acicular phases were virtually undetectable in the bottom region with 30% amplitude ultrasound, contrasting with their substantial presence without ultrasound. Figure 11f displays that larger brittle phases were also observed in the middle region at 80% amplitude again attributable to ultrasonic heat effect.

As evidenced in Figure 12, the presence of Al_4C_3 was nearly absent in the weld center following Ti addition. Severe agglomeration of TiC particles was observed without ultrasonic vibration, as shown in Figure 12a. With the application of ultrasonic vibration energy, a more dispersed distribution of TiC phase was found, and agglomeration was effectively mitigated, as demonstrated in Figures 12b,c. Wang et al. indicated that the cavitation effect generated by ultrasonic vibration can effectively refine the grain size, and the shock wave generated can disperse the segregated strengthening phase. At the same time, the acoustic flow effect promoted the uniform distribution of the strengthening phase (Wang et al., 2023b).

3.4 Metallurgical control mechanism and mechanical properties of aluminum matrix composite welded joints

In order to further clarify the metallurgical reaction mechanism inside aluminum based composite materials, this section analyzes from a thermodynamic perspective whether the base material and reaction products can be stable. Laser welding of SiCp/Al composites with a Ti interlayer involves complex metallurgical interactions: Ti interlayer melting, alloying with the Al matrix and SiC reinforcement, and subsequent reaction-recrystallization processes. The primary challenge remains the SiC-Al reaction that forms brittle Al_4C_3. This phase undergoes hydrolysis in humid environments, generating corrosion pits that serve as crack initiation sites under tensile stress. These defects create localized weak zones that severely compromise joint mechanical performance.

The addition of active elements Ti can partially or completely suppress Al4C3 formation. However, Ti addition introduces TiC and AlTi phases within the weld. The metallurgical reactions occurring in the molten pool are expressed by Equations 1–6 in Figure 13. Furthermore, based on the thermodynamic fundamentals established by Zhang et al. (2022b), the Gibbs free energy versus temperature curves for these metallurgical reactions were obtained (Guo et al., 2012). Silicon carbide decomposition in the molten pool proceeds via two pathways: direct decomposition under the high-energy laser beam (SiC→ Si + C), and dissolution-precipitation decomposition within the high-temperature melt. As shown in Figure 13, the ΔG values for reactions (2–6) were negative, indicating their spontaneous occurrence, while reaction (1) was an exception. At elevated temperatures, reaction (4) exhibits the highest propensity, signifying that TiC particle formation was most favorable. Although Al and C readily react to form Al_4C_3, this phase subsequently reacted with Ti via reaction (6) to form Al_3Ti and TiC phases. Consistent with findings in preceding sections, only

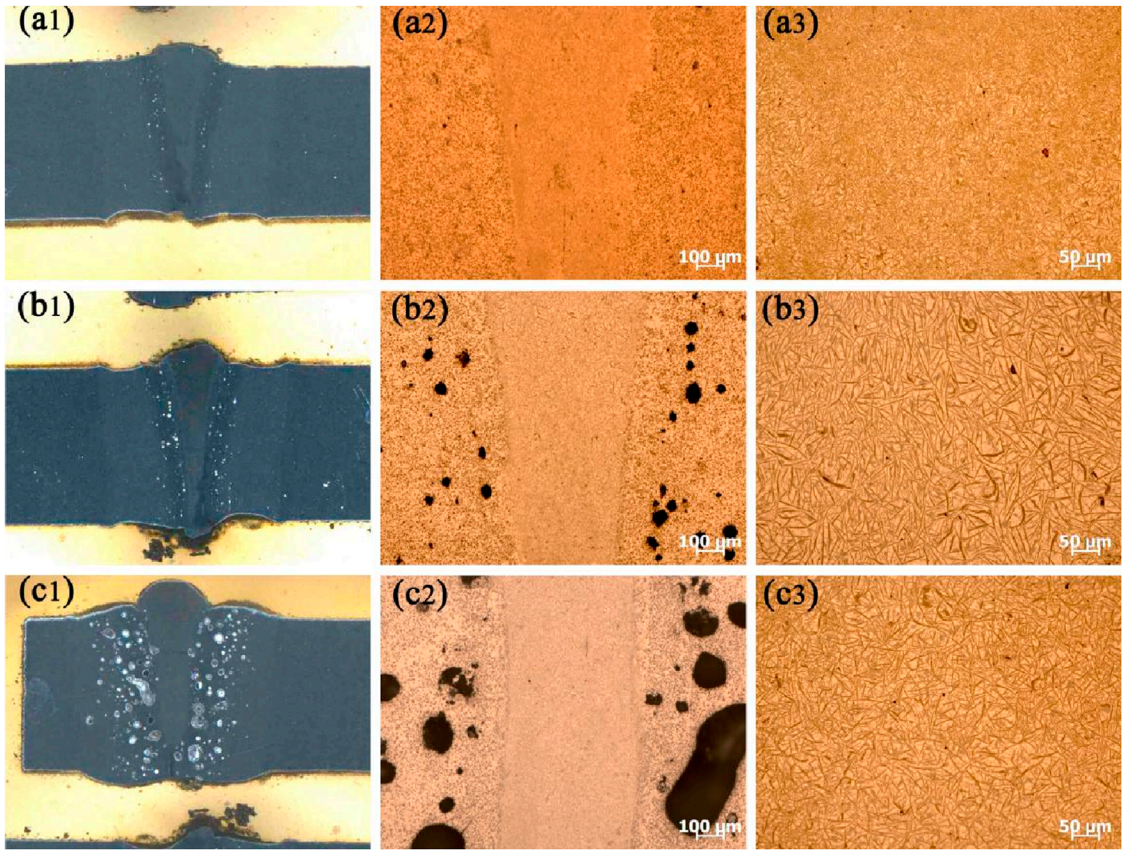

FIGURE 10
The SiCp/6092Al laser welded joint with different ultrasonic vibration **(a1~a3)** 30% ultrasonic amplitudes, **(b1~b3)** 50% ultrasonic amplitudes, **(c1~c3)** 80% ultrasonic amplitudes.

the TiC phase was detected in welds when limited Ti is present. This occurred because the available Ti reacted with C to form TiC, consuming only a portion of the carbon. The remaining carbon reacted with Al to form Al_4C_3, but insufficient Ti remained to react with and consume this Al_4C_3 via reaction (6).

Figure 14 illustrates the variation in tensile strength of laser-welded joints for aluminum matrix composites under different processing conditions. It was observed that for powder metallurgy-produced SiC/Al6092 composites, the joint tensile strength remained low regardless of the addition of active Ti foil. Without Ti, the direct laser welding strength was measured at only 58 MPa, increasing to 190 MPa with the addition of a 0.05 mm Ti foil, representing merely 41.6 percent of the base metal strength. Fracture in both conditions consistently occurred within the heat-affected zone (HAZ) adjacent to the weld seam. Conversely, for stir-casting SiC/Al6061 composites, the direct laser-welded joint strength reached 150 MPa. This strength was elevated to 260 MPa upon Ti foil addition, and a further increase to 286 MPa was achieved with the subsequent introduction of ultrasonic vibration at 30% amplitude, bringing the strength to 80.3 percent of the base metal value. However, a progressive decline in tensile strength was noted when the ultrasonic amplitude was increased to 50% and 80%, with the strength plummeting to only 60 MPa at 80% amplitude. This degradation was attributed to the significant porosity formed within the HAZ under these conditions, as confirmed by the data.

Figure 15 presents a schematic of these governing mechanisms in ultrasonic-assisted laser welding of SiCp/Al composite joints derived from microstructural analysis. During direct laser welding, brittle acicular Al_4C_3 phases are formed through reaction between reinforcing SiC phase and aluminum matrix. These phases exhibit marked susceptibility to hydrolysis, resulting in pit formation. Substantial residual stresses surrounding these hydrolysis pits and brittle phases are present, severely compromising joint mechanical properties (Li et al., 2023). Owing to titanium's higher carbon affinity compared to aluminum, its addition preferentially formed TiC particulate phases in the weld. Enhanced molten pool fluidity from titanium addition subsequently densifies the microstructure. This structural refinement substantially decreases defect formation (voids, porosity, lack of fusion) and promotes more uniform residual stress distribution. These aspects collectively underpin the tensile strength enhancement mechanism. However, the rapid cooling rate during laser welding induced TiC agglomeration due to titanium's limited diffusion distance. Applying an ultrasonic energy field effectively stirs the molten pool, dispersing active titanium uniformly and mitigating TiC clustering. The active titanium element further enhances reinforcement-matrix wettability and increase joint density. Ultrasonic vibration

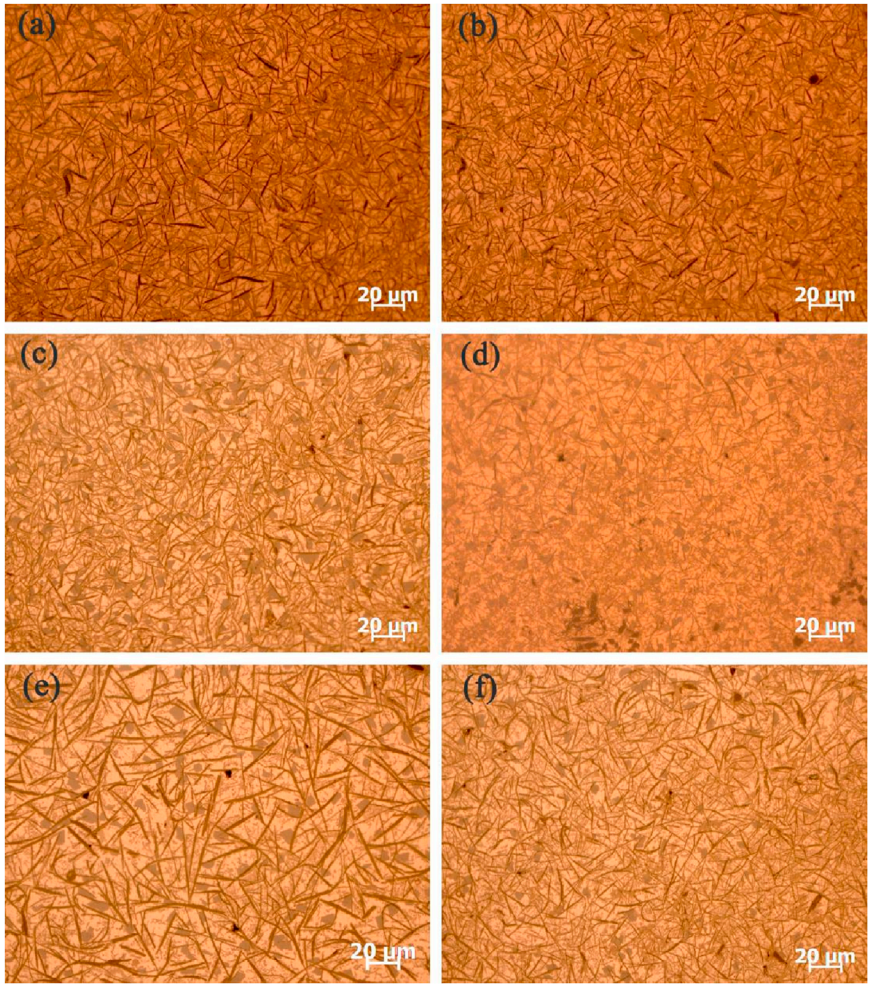

FIGURE 11
Al_4C_3 morphology in welds with different ultrasonic parameters, **(a)** and **(b)** the upper and middle weld regions under no ultrasound, **(c)** and **(d)** 30% amplitude, **(e)** and **(f)** 80% amplitude.

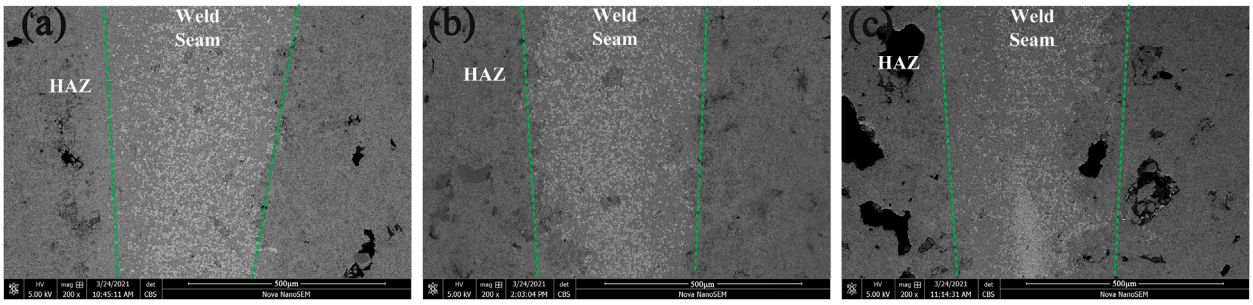

FIGURE 12
Distribution of strengthening phase in weld zone with different welding condition **(a)** no ultrasound, **(b)** 30% ultrasonic vibration, **(c)** 80% ultrasonic vibration.

during welding reduced both the inherent high viscosity of SiCp/Al melt pools and TiC segregation. This effect stems from three key mechanisms: cavitation-dominated melt flow enhancement, acoustic streaming-driven fluid motion, and acoustic radiation-induced particle redistribution (Zhang et al., 2020). Additionally, heat absorption during titanium melting reduces net welding heat input, which correlated with smaller Al_4C_3 phase dimensions.

Finally, an optimal range for ultrasonic energy input was determined. When excessive amplitudes were employed, such as

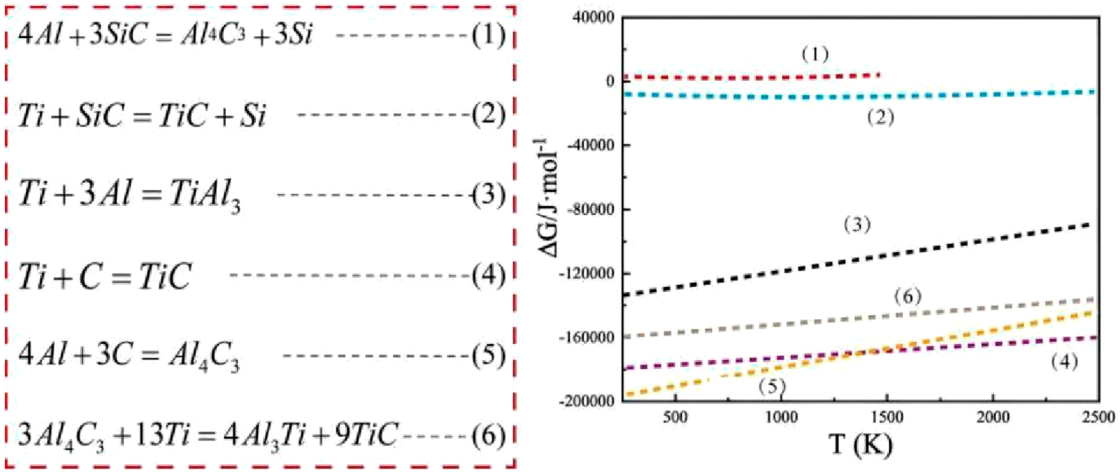

FIGURE 13
Gibbs free energy temperature curve of reaction products in laser welding of SiC/Al composite materials.

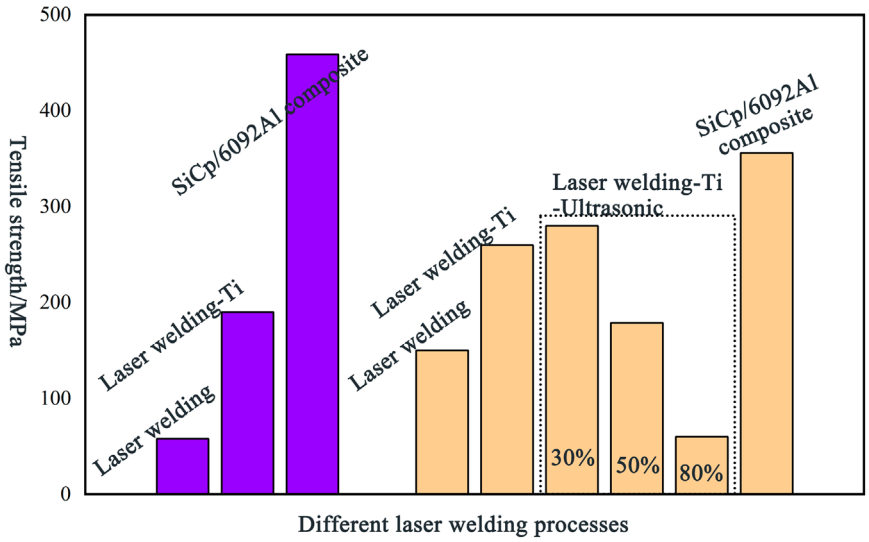

FIGURE 14
Tensile strength of laser-welded joints for aluminum matrix composites under different processing conditions.

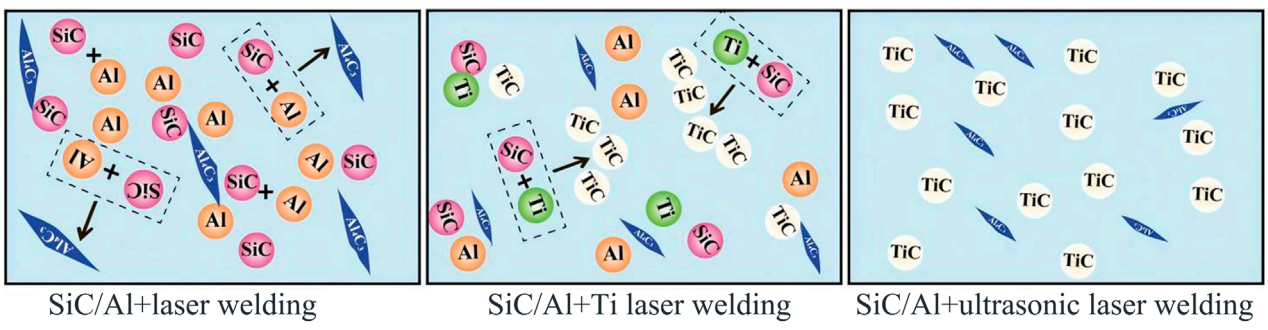

FIGURE 15
The operative mechanism for ultrasonic-assisted laser welding of SiCp/Al composite.

50% and 80% in this study, significant energy absorption by the molten pool occurred, prolonging the liquid metal holding time. This led to an increase in brittle phase size. Concurrently, the high amplitude induced substantial porosity formation within the HAZ of the welded joint. The combined effect of large brittle phases and porosity defects resulted in performance degradation, as evidenced by Figures 10, 13.

4 Conclusion

This study evaluated the laser weldability of two types of aluminum matrix composites using three advanced techniques: continuous laser welding, ultrasonic-assisted laser welding, and active interlayer application. The key findings were as follows:

1. Stir-casting SiCp/6061Al was demonstrated to exhibit superior laser weldability compared to powder metallurgy SiCp/6092Al, primarily attributable to significantly reduced porosity defects.
2. Incorporation of 0.05 mm titanium foil enabled preferential reaction with SiC to form TiC phases, thereby blocking the formation pathway of brittle Al_4C_3 intermetallics, which elevated the joint strength of SiCp/6061Al from 150 MPa to 260 MPa.
3. The 30% ultrasonic amplitude enhances molten pool fluidity through cavitation. This effect improves TiC dispersion while suppressing porosity and segregation, resulting in a joint strength of 286 MPa. Conversely, amplitudes above 50% cause pore resurgence from excessive heat input, which lowers strength to 60 MPa.
4. High-performance joining of stir-cast SiCp/6061Al is achieved through Ti foil with 30% ultrasonic-assisted laser welding, attaining 80% of base metal strength - providing a low-deformation solution for curved structural components such as monocoque bicycle frames.

Data availability statement

The original contributions presented in the study are included in the article/supplementary material, further inquiries can be directed to the corresponding authors.

Author contributions

XH: Writing – review and editing, Writing – original draft, Investigation. WZ: Formal Analysis, Writing – review and editing, Data curation, Writing – original draft. QZ: Writing – original draft, Writing – review and editing. WW: Validation, Supervision, Writing – review and editing, Resources, Writing – original draft.

Funding

The author(s) declare that financial support was received for the research and/or publication of this article. This work is supported by the Philosophy and Social Sciences Research of the Higher Education Institutions of Jiangsu Province, China (Grant No. 2023SIVB2161).

Acknowledgments

The authors would like to thank Hongyang Cao of the Materials Science and engineering Department of Jiangsu University for helpful discussions on topics related to this work.

Conflict of interest

The authors declare that the research was conducted in the absence of any commercial or financial relationships that could be construed as a potential conflict of interest.

Generative AI statement

The author(s) declare that no Generative AI was used in the creation of this manuscript.

Any alternative text (alt text) provided alongside figures in this article has been generated by Frontiers with the support of artificial intelligence and reasonable efforts have been made to ensure accuracy, including review by the authors wherever possible. If you identify any issues, please contact us.

Publisher's note

References

Barker, M. B., Davidson, A. M., and Regener, D. (2020). *Developments of manufacturing of metal matrix composites for applications in the sports and leisure industries[M]*. Boca Raton, FL: CRC Press, 153–160.

Chatterjee, A., Sen, S., Paul, S., Roy, P., Seikh, A. H., Alnaser, I. A., et al. (2023). Fabrication and characterization of SiC-reinforced aluminium matrix composite for brake pad applications. *Metals* 13 (3), 584. doi:10.3390/met13030584

Chen, S. (2024). Advancements in surface treatments for aluminum alloys in sports equipment. *Rev. Adv. Mater. Sci.* 63 (1), 20240065. doi:10.1515/rams-2024-0065

Ferraris, M., Gili, F., Lizarralde, X., Igartua, A., Mendoza, G., Blugan, G., et al. (2022). SiC particle reinforced Al matrix composites brazed on aluminum body for lightweight wear resistant brakes. *Ceram. Int.* 48 (8), 10941–10951. doi:10.1016/j.ceramint.2021.12.313

Gao, J., Tunio, M. H., Chen, Y., and He, R. (2020). Design and experiment of low-frequency ultrasonic nozzle integrating air-assistant system and acoustic levitation mechanism. *Int. J. Agric. Biol. Eng.* 13 (6), 25–33. doi:10.25165/j.ijabe.20201306.5419

Gao, Z., Zhang, J., Ba, X., Liu, Y., Huang, M., and Wang, P. (2025). Experimental study on the low-power laser-TIG hybrid welding of SiCp/6061-T6 Al matrix composites. *Opt. Lasers Eng.* 186, 108861. doi:10.1016/j.optlaseng.2025.108861

Guo, J., Gougeon, P., and Chen, X. (2012). Study on laser welding of AA1100-16 vol.% B4C metal–matrix composites. *Compos. Part B Eng.* 43 (5), 2400–2408. doi:10.1016/j.compositesb.2011.11.044

Gupta, P. K., Trivedi, A. K., Gupta, M. K., and Dixit, M. (2024). Metal matrix composites for sustainable products: a review on current development. *Proc. Institution Mech. Eng. Part L J. Mater. Des. Appl.* 238 (10), 1827–1864. doi:10.1177/14644207241238197

Han, R., Li, X., and Peng, Y. (2024). Effect of hot extrusion of SiCp/2024Al composites on microstructure and properties of laser welded joint. *Acta Armamentarii* 45 (6), 2054. doi:10.12073/j.hjxb.20201003002

Han, K., Cao, Y., Han, R., Li, X., Feng, Y., Liu, J., et al. (2025). Effect of TiB2/2024Al composite filler on the microstructure and mechanical properties of SiCp/2024Al composites welded joint by laser welding. *Mater. Charact.* 228, 115344. doi:10.1016/j.matchar.2025.115344

Hao, G., Shi, C., Zhao, N., Liu, E. Z., He, C. N., He, F., et al. (2023). Microstructural evolution and mechanical behavior of *in situ* synthesized MgAl2O4 whiskers reinforced 6061 Al alloy composite after hot extrusion and annealing. *Rare Met.* 42 (5), 1732–1742. doi:10.1007/s12598-018-1119-6

Hua, Z., Xiang, Y., Wang, C., Jiang, P., Zhang, M., Hu, Y., et al. (2024). Investigation of Ti alloying for microstructural evolution and strengthening mechanism: avoiding Al4C3 formation in SiCp/Al composites via laser directed energy deposition. *J. Alloys Compd.* 970, 172371. doi:10.1016/j.jallcom.2023.172371

Huang, Y., Xie, Y., Chen, J., Li, J., Zhao, Y., and Meng, X. (2025). Wire-based friction stir additive remanufacturing of 2219 aluminum alloy components. *Int. J. Adv. Manuf. Technol.* 137 (11), 6029–6041. doi:10.1007/s00170-025-15544-5

Kesharwani, R., Jha, K. K., Imam, M., and Sarkar, C. (2024). Selection of groove dimension in the fabrication of particulate reinforced aluminium matrix composites using friction stir welding. *Mater. Lett.* 367, 136640. doi:10.1016/j.matlet.2024.136640

Leng, B., Xue, Y., Li, J., Qi, J., Yi, A., and Zhao, Q. (2024). A critical review of anti-corrosion chemical surface treatment of aluminum alloys used for sports equipment. *Crystals* 14 (1), 101. doi:10.3390/cryst14010101

Li, H., Cao, H., Zhu, Q., Lu, Y., Wang, Z., Zhao, W., et al. (2021). Influence of welding process on microstructure and properties of laser welding of SiCp/6061 Al matrix composite. *Front. Mater.* 8, 779324. doi:10.3389/fmats.2021.779324

Li, H., Cao, H., Xia, H., Han, K., Wang, Z., Wang, D., et al. (2023). Effects of laser power on the microstructural evolution and mechanical performance in laser dissimilar welding of TC4 to SiCp/6092Al composite. *Mater. Charact.* 206, 113391. doi:10.1016/j.matchar.2023.113391

Li, C., Ping, Z., Qi, E., and Wu, S. (2025). Wire oscillating laser butt welding of SiCp/2009Al metal-matrix composite sheets with preseted gap there between. *Weld. World*, 1–14. doi:10.1007/s40194-025-02059-6

Linjie, L., Quanwei, C., Jianxing, Z., Wenlei, S., Zhicheng, L., Haoran, S., et al. (2024). Research on the temperature rise mechanism of ultrasonic field-assisted laser cladding. *Int. J. Material Form.* 17 (6), 56. doi:10.1007/s12289-024-01859-3

Liu, J., Zhu, H., Li, Z., Cui, W., and Shi, Y. (2019). Effect of ultrasonic power on porosity, microstructure, mechanical properties of the aluminum alloy joint by ultrasonic assisted laser-MIG hybrid welding. *Opt. & Laser Technol.* 119, 105619. doi:10.1016/j.optlastec.2019.105619

Lu, Y., Xu, W., Leng, J., Liu, X., Xu, H., Ding, H., et al. (2024). Review and research prospects on additive manufacturing technology for agricultural manufacturing. *Agriculture* 14 (8), 1207. doi:10.3390/agriculture14081207

Madhu, K. S., Sharath, B. N., and Karthik, S. (2025). *An introduction to metal matrix composites and their applications*. Elsevier, 45–73.

Meng, X., Huang, Y., Cao, J., Shen, J., and dos Santos, J. F. (2021). Recent progress on control strategies for inherent issues in friction stir welding. *Prog. Mater. Sci.* 115, 100706. doi:10.1016/j.pmatsci.2020.100706

Mi, G., Liu, C., Wang, C., Xiong, L., and Ouyang, Q. (2021). The effect of Zr addition on the laser welding of SiCp/2A14Al composite. *J. Mater. Res. Technol.* 15, 5175–5186. doi:10.1016/j.jmrt.2021.10.097

Ndukwe, A. I. (2023). Recent findings on mechanical behaviour of stir cast aluminium alloy-matrix composites: an overview. *Acta Period. Technol.* (54), 223–235. doi:10.2298/apt2354223n

Pan, P., Wang, J., Chen, S., Tao, W., Wang, Y., Yin, Q., et al. (2024). Effect of filler metal on microstructure and mechanical properties of welded SiCp/Al composites by dual beam laser welding. *Mater. Lett.* 372, 136984. doi:10.1016/j.matlet.2024.136984

Sharma, A. K., Bhandari, R., and Pinca-Bretotean, C. (2021). A systematic overview on fabrication aspects and methods of aluminum metal matrix composites. *Mater. Today Proc.* 45, 4133–4138. doi:10.1016/j.matpr.2020.11.899

Singh, H., Brar, G. S., Kumar, H., and Aggarwal, V. (2021). A review on metal matrix composite for automobile applications. *Mater. Today Proc.* 43, 320–325. doi:10.1016/j.matpr.2020.11.670

Sun, S., Zheng, L., Liu, J., and Zhang, H. (2023). Microstructure, cracking behavior and control of Al–Fe–V–Si alloy produced by selective laser melting. *Rare Met.* 42 (4), 1353–1362. doi:10.1007/s12598-016-0846-9

Wang, Z., Cao, H., Li, H., Wang, D., Xia, H., Butt, H. A., et al. (2023a). Effects of laser welding parameters on the porosity and acicular phase in SiCp/6092 aluminum matrix composite welded joints. *J. Mater. Res. Technol.* 23, 5127–5141. doi:10.1016/j.jmrt.2023.02.153

Wang, J., Zhou, J., Zhang, T., Meng, X., Li, P., Huang, S., et al. (2023b). Ultrasonic-induced grain refinement in laser cladding nickel-based superalloy reinforced by WC particles. *Coatings* 13 (1), 151. doi:10.3390/coatings13010151

Wang, Y., Huang, F., and Qian, X. (2025). MoTiCo conversion coating on 7075 aluminium alloy surface: preparation, corrosion resistance analysis, and application in outdoor sports equipment trekking poles. *Metals* 15 (8), 864. doi:10.3390/met15080864

Xie, Y., Dong, J., Wu, L., Wang, W., Sun, X., Meng, X., et al. (2025). Unraveling the relationship between severe plastic deformation and corrosion responses of AZ31 Mg alloys. *Corros. Sci.* 250, 112881. doi:10.1016/j.corsci.2025.112881

Zhang, M., Zhao, G. L., Wang, X. H., Liu, S., and Ying, W. (2020). Microstructure evolution and properties of *in-situ* ceramic particles reinforced Fe-based composite coating produced by ultrasonic vibration assisted laser cladding processing. *Surf. Coatings Technol.* 403, 126445. doi:10.1016/j.surfcoat.2020.126445

Zhang, M., Wang, C., Mi, G., and Ouyang, Q. (2022a). *In situ* study on fracture behaviors of SiC/2A14Al composite joint: co-construction of microstructure and mechanical properties via laser welding. *Compos. Part B Eng.* 238, 109882. doi:10.1016/j.compositesb.2022.109882

Zhang, M., Wang, C., Mi, G., Jiang, P., and Zhang, X. (2022b). *In-situ* formation Ti-Al-C compounds reinforced SiCp/2A14 Al joint: microstructure evolution and mechanical properties. *Opt. & Laser Technol.* 150, 107896. doi:10.1016/j.optlastec.2022.107896

Zhang, M., Wang, C., Hua, Z., Hu, Y., Ouyang, Q., and Mi, G. (2023a). Microstructure evolution, interface and mechanical properties of SiCp/2A14 joint during laser keyhole welding. *J. Mater. Res. Technol.* 26, 5731–5747. doi:10.1016/j.jmrt.2023.08.240

Zhang, M., Wang, C., Zeng, G., Ouyang, Q., and Mi, G. (2023b). L12-(Al, Si) 3Ti+ TiC hybrids reinforced laser welded SiCp/2A14Al joint with extraordinary strength. *Mater. Charact.* 205, 113295. doi:10.1016/j.matchar.2023.113295

Zhang, S., Zhao, L., Zhao, M., Liu, D., and Song, L. (2024a). Microstructure and interfacial behavior of SiCp/6061 aluminum matrix composite joined by laser welding with filled Ti x Si powder. *J. Mater. Sci.* 59 (40), 18848–18863. doi:10.1007/s10853-024-09770-7

Zhang, M., Wang, C., Mi, G., Zhai, C., and Li, J. (2024b). Dispersion of reinforcing micro-particles in the laser welding of metal matrix composites: high-fidelity modeling with experimental characterization. *Mater. Charact.* 207, 113561. doi:10.1016/j.matchar.2023.113561

Zhang, B., Mi, G., Zhang, M., Jiang, Y., Ouyang, Q., and Zeng, G. (2024c). Research on the laser welding process and performance analysis of SiCp/Al composite and 2A14 aluminum alloy dissimilar metals. *J. Manuf. Process.* 125, 239–252. doi:10.1016/j.jmapro.2024.06.025

Zhou, H., and Zhang, Z. (2023). Evolution of silicon particle damage on fatigue crack initiation and early propagation in an aluminum alloy. *Rare Met.* 42 (7), 2470–2476. doi:10.1007/s12598-017-0930-9

Zhu, Q., Zhao, W., and Lei, Y. (2021). Effect of Ti on microstructure and properties of laser welding weld of SiC particle reinforced 6092 Al alloy matrix composite. *Trans. China Weld. Institution* 42 (3), 85–90. doi:10.12382/bgxb.2023.0105